SkinLumina: Inclusive Multispectral Skin Analysis Device

Tatiana Cutrone, Ryan Rodriguez, Tiffany Thani, Abdullah Al-Gharabally

CREOL, The College of Optics and Photonics, University of Central Florida, Orlando, Florida 32816-2450

Dept. of Electrical Engineering and Computer Science, University of Central Florida, Orlando, Florida, 32816-2450

***Abstract* — SkinLumina is a portable multispectral imaging system developed to improve inclusivity in dermatological analysis by adapting to diverse skin types. Unlike conventional imaging tools affected by calibration bias, it dynamically adjusts illumination and exposure parameters for accurate imaging across pigmentation levels. The system integrates visible and near-infrared (NIR) LEDs, a motorized filter wheel, achromatic optics, and cross-polarization to capture surface and subsurface skin features. Real-time firmware control synchronizes image acquisition and brightness calibration, enabling high-fidelity, non-invasive imaging that supports early detection and equitable clinical assessment.**

***Index Terms* — Biomedical imaging, dermatology, multispectral imaging, skin, image calibration, optical system design, photonics, human factors**

I. Introduction

Dermatological imaging plays a critical role in detecting and diagnosing skin conditions such as melanoma, scars, and other abnormalities. Although optical and computational imaging technologies have advanced rapidly, many existing systems still do not perform reliably across the full range of human skin tones. Most imaging devices are calibrated using standard skin models that represent lighter complexions, which introduces bias and reduces diagnostic accuracy for individuals with higher melanin concentrations. As a result, early signs of skin disease in people with darker skin are often more difficult to detect because current systems lack the sensitivity and adaptability needed for inclusive analysis. Developing an imaging system that accounts for the optical diversity of human skin is therefore an essential step toward achieving more equitable and consistent dermatological evaluation.

Motivation — The goal of the SkinLumina project is to design an imaging device that promotes inclusivity through optical adaptability. The way light interacts with skin depends strongly on the presence of melanin, hemoglobin, and the structure of the tissue layers. Shorter visible wavelengths are strongly absorbed by melanin, which makes it difficult to image deeper features in darker skin. In contrast, longer near infrared wavelengths penetrate deeper into the dermis but may lose information from the surface. SkinLumina uses both visible and infrared wavelengths to create balanced and high contrast imaging for every skin type. It also adjusts its illumination and exposure automatically based on an initial baseline scan so that the captured reflectance remains consistent and clear for any skin tone.

Problem Statement — Current imaging systems are either large and expensive or lack the ability to adapt spectrally and optically to different patients. These limitations result in inconsistent performance, diagnostic bias, and limited use outside clinical environments. A small, energy efficient multispectral system capable of real time calibration and glare reduction is needed to close this technological and clinical gap.

Objectives — SkinLumina is designed to capture both surface and subsurface skin features using visible and infrared light, optical filtering, and polarization control. The system integrates hardware and software to provide accurate, noninvasive imaging while remaining within safe light exposure limits. The ultimate goal is to support dermatological evaluation that is consistent, equitable, and reliable for all people.

II. System Design Overview

The SkinLumina system operates through a two-stage imaging process that combines baseline calibration with multispectral data acquisition. In the first stage, a white-light baseline scan records the subject's skin reflectance profile, which is then used to automatically adjust illumination intensity, exposure, and gain settings. The second stage performs wavelength specific imaging using visible and near-infrared light to capture both surface and subsurface skin information. Together, these stages enable adaptive imaging that maintains

consistent contrast and clarity across different skin tones.

The design is composed of four primary subsystems: optical imaging, spectral illumination, electronic control, and software management. Each part of the system is engineered for precision alignment, compact operation, and safety compliance.

A. Optical System Architecture

The optical system provides high resolution imaging across visible and near infrared wavelengths. It includes a CMOS image sensor, polarization optics, achromatic relay and objective lenses, a variable aperture, and a motor driven filter wheel. Cross polarization reduces glare and enhances subsurface visibility, while the achromatic lenses minimize both chromatic and spherical aberrations. The adjustable aperture controls numerical aperture and contrast, and the filter wheel selects wavelength bands that are synchronized with the illumination source. The optical assembly maintains alignment within a tolerance of one tenth of a millimeter to ensure accurate focus and consistent calibration.

B. Illumination and Spectral Filtering

The housing unit functions as a Lambertian reflector, providing diffuse, uniform illumination across the imaging field. A circular white LED ring surrounds the sample and is angled at twenty degrees toward the skin to create balanced lighting for the baseline scan. During the multispectral scan, visible and near infrared LEDs positioned outside the white ring are angled at thirty degrees to enhance depth sensitivity. A motor driven filter wheel contains wavelength specific filters matched to each LED. As images are captured, the wheel rotates to block inactive sources and isolate each illumination band for precise spectral imaging.

C. Electronic Control Subsystem

The control electronics manage all functions of the system through a two controller arrangement. A Raspberry Pi computer oversees image acquisition, data storage, and the user interface, while an Arduino microcontroller controls light modulation, motor positioning, and timing coordination. Power is supplied through a twelve volt regulated source that includes protection circuits for current and voltage stability.

D. Software and Control Interface

The SkinLumina control software operates through three main stages: capture, analyze, and display. During the *capture* stage, the Raspberry Pi activates the selected LED wavelength and synchronizes the camera to acquire an image under controlled illumination. The *analyze* stage processes the captured data by sampling the central region of the image to extract RGB and hexadecimal color values, which represent the user's skin reflectance profile. These values are used to evaluate color balance and determine any needed adjustments to the LED brightness or spectral weighting for the next capture cycle.

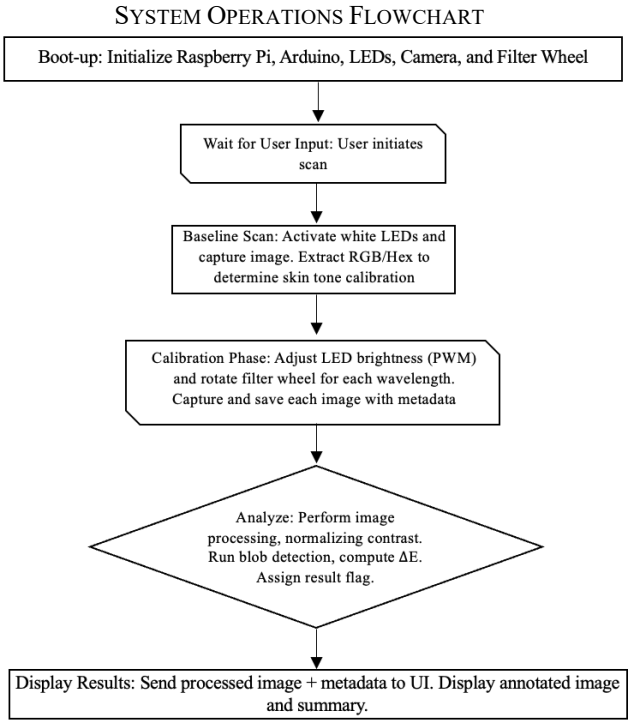

Fig. 1. Complete SkinLumina system flowchart illustrating the sequential flow between three major operation states — capture, analyze, and display.

In the *display* stage, the processed image and calculated reflectance data are shown on the user interface. The interface provides real-time visual feedback, allowing the user to view skin images taken at multiple wavelengths and observe contrast variations between spectral bands. This continuous sequence: capture, analyze, and display as shown in figure 1. This enables SkinLumina to dynamically adapt illumination, optimize image quality, and maintain consistent spectral calibration across a wide range of skin tones.

III. System Components

The SkinLumina imaging device integrates optical, electrical, and computational subsystems into a compact multispectral platform. The major system components and their functions are summarized below.

A. Raspberry Pi 4 (Model B)

Acts as the central processing and control unit. It executes all Python-based operations, synchronizes LED illumination with image capture, manages the motorized filter wheel, and processes image data for adaptive calibration. This is labelled and shown a part of the MCU in the system optical schematic in figure 2.

Optical Schematic of the Imaging System

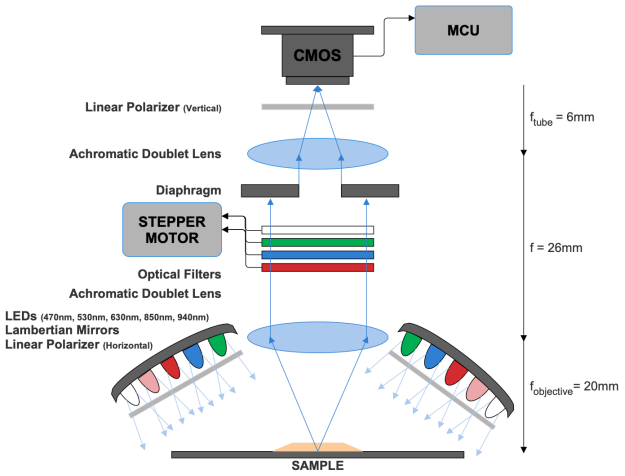

Fig. 2. Schematic layout of the SkinLumina optical path with major components labeled. Illumination from the multispectral LED array passes through wavelength filters, reflects off the skin sample, and is focused onto the CMOS sensor by the objective and tube lenses. The polarizer, filter wheel, and 3D-printed housing reduce glare, isolate spectral bands, and maintain alignment for high-quality imaging.

B. CMOS Camera Module

The imaging system uses a Sony IMX219 CMOS camera module chosen for its low cost, small size, and low power use. The 2-megapixel sensor meets system resolution needs and is sensitive to both visible and near-infrared light. It captures clear images across multiple wavelengths without requiring cooling or high-power circuitry. The module connects directly to the Raspberry Pi, providing RGB data for reflectance analysis and adaptive illumination control, making it ideal for portable multispectral imaging.

C. Multispectral LED Array

Provides illumination at six wavelengths: 470, 525, 630, white (broadband), 850, and 940 nm. Each wavelength reaches different tissue depths, allowing both surface and subsurface imaging. The visible and near-infrared bands lie within the 600–1300 nm therapeutic window, where reduced absorption by melanin and hemoglobin enables deeper, clearer imaging.

D. LED Driver Circuit and Buck Converter

Regulates voltage and current to each LED channel. The LM2678 converter efficiently steps the 12-volt input down to 5 volts, maintaining consistent brightness and preventing thermal instability.

E. Motorized Filter Wheel

Holds wavelength-specific optical filters that correspond to each LED channel. The wheel rotates under software control to align the correct filter with the optical path during image acquisition, isolating the active wavelength and improving spectral accuracy. This is located in the system in figure 2 labelled as the stepper motor between the lens assembly and before the CMOS camera module.

Visible narrowband filters (±10 nm) were selected to isolate individual LED wavelengths and minimize spectral overlap. Optical density 4 filters provide strong blocking of unwanted light, achieving transmission levels as low as 0.0001 outside the target band. Each filter is 12.5 mm in diameter, chosen to fit the compact system geometry, and mounted in a filter wheel that allows rapid wavelength switching and precise spectral selection during imaging.

F. Linear Polarizer

Positioned in front of the camera lens to reduce specular reflection and surface glare from the skin. The polarizer improves image contrast by enhancing detection of diffusely reflected and subsurface light.

G. Achromatic Lens Assembly

Achromatic doublet lenses are used for both the objective and tube lens to minimize chromatic aberrations across the visible and near-infrared LED bands. The objective lens is designed for a short working distance and high optical clarity, ensuring accurate focus of both surface and subsurface skin features during imaging. The

tube lens provides the proper magnification and optical coupling between the objective and the CMOS sensor, enabling full field image capture without distortion or vignetting. Both lenses feature broadband anti-reflective coatings optimized for 400 to 1000 nanometers, reducing reflection losses and improving illumination efficiency across all operational wavelengths.

ZEMAX LENS RAY PATH DIAGRAM

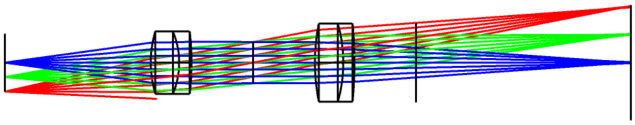

Fig. 3. Ray-trace diagram of the SkinLumina optical system modeled in Zemax.

In the figure 3 Zemax ray diagram, the objective plane is positioned on the left, where illumination from the LED array reflects off the skin sample and is directed through the two selected lenses before forming the image at the imaging plane located on the right side of the system.

H. Housing Unit

A Custom 3D-Printed housing unit holds and aligns the optical components in a stable configuration. The interior surface acts as a Lambertian reflector to promote uniform light distribution across the skin sample while maintaining a fixed working distance.

I. Power Supply and Regulation System

The SkinLumina system is powered by a $LiFePO_4$ battery source that provides a stable and safe energy supply for portable operation. The power distribution network delivers a 12-volt output for the motorized filter wheel and a regulated 5-volt output for the LED array, MCU, and Raspberry Pi board. All subsystems share a common ground to ensure consistent reference levels and minimize electrical noise across the circuit.

SYSTEM POWER REGULATION CIRCUIT

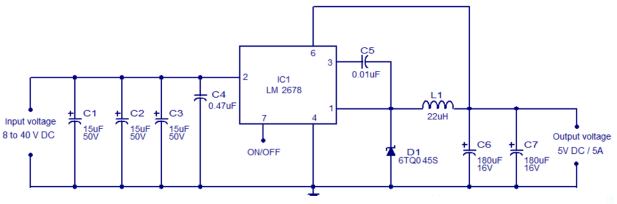

Fig. 4. Circuit diagram showing the 12V power input, LM2678 buck converter, and regulated 5V and 12V outputs supplying the MCU, Raspberry Pi, LED array, and motorized components.

Voltage regulation is achieved using the LM2678 integrated circuit as seen in the center of the circuit shown in figure 4. A high-efficiency buck converter steps the 12-volt input down to a steady 5-volt output with an efficiency of up to 92 percent. This converter provides a reliable, cool-running 5-ampere output suitable for powering sensitive components while preventing overheating or instability.

J. Adaptive Imaging Control Software

The software and control interface form the adaptive core of the SkinLumina system. Its primary function is to dynamically adjust LED brightness based on the user's unique skin reflectance profile. Each image captured by the camera is analyzed at its center pixel to extract RGB and hexadecimal color values, which are used to evaluate skin tone reflectivity across spectral channels.

Using this feedback, the Raspberry Pi modifies the LED driver outputs to balance illumination for subsequent image captures as seen in table I. If the system detects reduced reflectance in a particular color channel, the corresponding LED intensity is increased to improve contrast and signal uniformity. This adaptive loop continuously refines illumination across the red, green, blue, and near-infrared wavelengths, providing consistent imaging performance for different pigmentation levels and lighting conditions.

TABLE I
LED CHANNEL CALIBRATION BEHAVIOR BASED ON SKIN-TONE PROFILE

Skin Tone Profile	Dominant Color Traits	LED Adjustment Strategy	Expected Effect
Low Reflectance (Deep Tone)	Lower red, green, and blue intensity	Increase red brightness, slightly boost green, reduce blue	Enhances contrast and surface visibility
Medium Reflectance (Neutral Tone)	Balanced red, green, and blue values	Maintain equal LED intensity across channels	Preserves natural color representation
High Reflectance (Light Tone)	Higher red and blue reflectance	Dim red output, increase green and blue illumination	Prevents oversaturation and balances lighting

System Firmware — The SkinLumina software is written in Python and runs on a Raspberry Pi 4. It serves as the main control system for image capture, LED sequencing, and image analysis. The software communicates with external modules through serial and network connections, coordinating hardware control with data processing. The main program initializes all system components, sets the camera and

LED parameters, and then runs a sequence of functions to manage the imaging process.

FIRMWARE PROGRAM LOOP

```
initialize_camera()
configure_LEDs()
while (system_active):
        capture_image()
        analyze_image()
        log_metadata()
        transmit_results()
```

Fig. 5. Simplified main program loop of the SkinLumina firmware.

(1) initialize_camera(): Establishes communication with the Pi Camera module, sets resolution and exposure, and synchronizes timestamps for consistent image logging.
(2) configure_LEDs(): Sets initial current and brightness levels for each wavelength. LED output is dynamically adjusted based on analysis feedback to maintain uniform illumination across skin tones.
(3) capture_image(): Triggers image acquisition using the *rpicam-still* utility and saves each image locally with a unique timestamp and identifier.
(4) analyze_image(): Performs hex-code color mapping and edge detection. Color mapping converts pixels to hexadecimal RGB values, while edge detection isolates lesion boundaries and enhances contours using adaptive thresholding.
(5) log_metadata(): Records ΔE color deviation, boundary sharpness, and processing time. Data are stored in a CSV file with timestamps, wavelength, and image parameters.
(6) transmit_results(): Sends raw and annotated images with metadata to the Node/Express backend through a REST API for database storage and web visualization.

Embedded Control and Synchronization — SkinLumina uses an embedded communication link between the Raspberry Pi and Arduino to coordinate LED control, filter-wheel movement, and image timing. The Pi sends LED intensity and filter position data, which the Arduino uses to adjust brightness via PWM and rotate the filter wheel. Once aligned, the Arduino signals the Pi to capture the next image. This cycle repeats across all wavelengths, maintaining precise synchronization between illumination and imaging.

SERIAL COMMUNICATION AND IMAGE CAPTURE

```
read_center_hex()
    ➔ compute_LED_adjustments()
    ➔ send_serial_command()
    ➔ wait_for_acknowledgment
    ➔ capture_image()
    ➔ repeat_across_all_filters()
```

Fig. 6. Serial communication sequence between Raspberry Pi and microcontroller for LED modulation, filter-wheel rotation, and synchronized image capture.

Each iteration is time-stamped and verified to prevent overlap or skipped frames. This ensures consistent spectral illumination, mechanical accuracy, and reproducible imaging conditions across sessions.

IV. METHODS AND EXPERIMENTAL SETUP

The SkinLumina prototype was assembled and tested to evaluate imaging accuracy, calibration stability, and optical safety. The housing was 3D printed for precise placement of optical components, and all lenses, filters, and the illumination array were aligned concentrically with the imaging axis to ensure uniform illumination. Electrical and control elements were mounted on a custom PCB connecting the LEDs, camera, and stepper motor to the dual microcontroller system.

Before each imaging session, a white-light baseline scan established the subject's reflectance profile and calibrated exposure, gain, and LED brightness. Calibration was verified using a neutral reflectance standard, and all light sources operated below the IEC 62471 safety limit of ten milliwatts per square centimeter.

Synthetic skin phantoms were made from Smooth-On Dragon Skin 20 silicone with titanium dioxide for scattering, Higgins India Ink for absorption, and Silc-Pig pigments for skin tone variation. Samples representing light, medium, and dark complexions demonstrated optical properties comparable to biological skin.

During imaging, each phantom or subject was placed five centimeters below the imaging head. The white LED ring provided the initial reflectance map, followed by sequential captures through wavelength-specific filters at 470, 530, 630, 850, and 940 nanometers. Temperature remained stable within three degrees Celsius of ambient through efficient power regulation and heat dissipation. Repeated tests confirmed stable alignment, uniform illumination, and precise synchronization, validating the calibration process and the silicone phantoms as accurate optical models for inclusive skin imaging.

V. Data Analysis and Results

A series of experiments were performed to evaluate the performance and reliability of the SkinLumina system. Each subsystem was tested to verify design accuracy, calibration stability, and overall integration. The following sections summarize key findings that demonstrate the system's consistent optical, electrical, and computational performance for inclusive and repeatable skin imaging.

A. Buck Converter Efficiency Testing

A buck converter, also called a step-down DC to DC converter, is a key part of the power subsystem. This reduces the input voltage from 12 volts to a regulated 5 volt output. A conversion is needed to power key electronic components such as the LED arrays, the CMOS imaging sensor, and the microcontroller while maintaining voltage stability. Using a buck converter, as seen in figure 1, minimizes power loss and ensures thermal safety for the system. The converter's performance directly affects the overall device reliability and the optical output consistency due to voltage instability. Voltage instability can cause illumination flickering, image noise, or sensor error.

Buck Converter PCB Layout

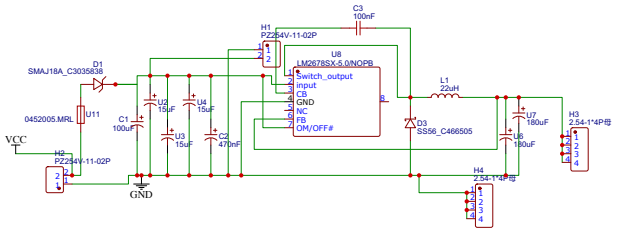

Fig. 7. Power regulation printed circuit board schematic.

Evaluating the efficiency and stability of the LM2678 converter used, is an important step in confirming that the electrical design of the system will perform as intended. The layout in figure 7 shows optimized trace routing for current flow, heat control, and low electrical noise between the 12 volt input and 5 volt output stages.

Data Analysis — To measure the performance of the LM2678 buck converter used, the assembled PCB was connected to a DC electronic load machine. This setup simulated the different output current levels, while keeping the input at a constant 12 volts. The output current was increased in controlled steps of 0.5 ampere, 1.0 ampere, 1.5 amperes, and 2.0 amperes. At each level, both input and output voltages and currents were measured using calibrated multimeters, and the power was calculated using the equation

$$P=V\times IP=V\times I \tag{1}$$

The converter efficiency, represented by the Greek letter η, was then calculated for each step using the formula

$$\eta = \frac{V_{out} \times I_{out}}{V_{in} \times I_{in}} \times 100 \tag{2}$$

This method allowed a clear view of the LM2678 converter's performance as the current demand increased. Monitoring efficiency over several load steps helped identify switching losses, conduction losses, and voltage stability. [1]

TABLE II
Buck Converter Test Parameters

Load (A)	V_{in} (V)	I_{in} (A)	P_{in} (W)	V_{out} (V)	I_{out} (A)	P_{out} (W)	Efficiency (%)
0.5	12.00	0.27	3.240	4.80	0.50	2.400	74.07
1.0	12.00	0.52	6.240	4.60	1.00	4.600	73.72
1.5	12.00	0.82	9.840	4.50	1.50	6.750	68.60
2.0	12.00	1.12	13.440	4.30	2.00	8.600	63.99

The measured input and output parameters for the buck converter test performed was used in equation (2) to calculate the conversion efficiency shown in table II.

Results — The measured data was used to generate the converter efficiency profile as a function of output current, shown in figure 8.

Buck Converter Efficiency vs. Output Current

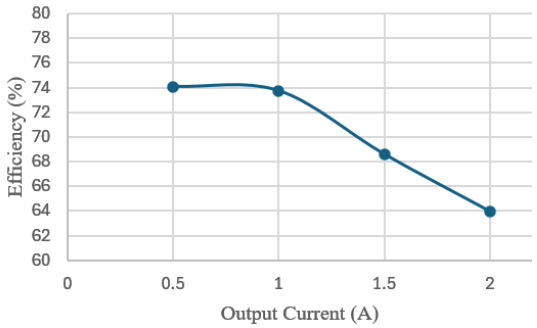

Fig. 8. The measured data was used to generate the converter efficiency profile as a function of output current.

The converter achieved an efficiency of about 74 percent under lighter loads from 0.5 to 1.0 ampere and

gradually decreased to about 64 percent at the maximum load of 2.0 amperes. This trend matches expected behavior for DC to DC converters, where higher current causes increased switching and conduction losses. Even with this decline, the LM2678 maintained stable output regulation with the voltage decreasing only from 4.8 volts to 4.3 volts as the load increased.

Conclusions — No oscillations, voltage instability, or overheating were observed during the test sequence. This confirmed that the power regulation circuit on the SkinLumina printed circuit board operates safely and consistently. The converter's stable performance across multiple load levels validates the electrical design's ability to provide continuous power for the optical and control subsystems. Reliable power delivery supports consistent LED illumination and image capture, which are essential for maintaining accuracy in multispectral imaging.

B. LED Illumination Profile Characterization

To verify the spectral accuracy and stability of the SkinLumina illumination system, each LED in the multispectral array was individually tested to confirm its emission wavelength, optical output consistency, and alignment with the system's designed imaging bands. The LED array forms the foundation of the device's multispectral operation by providing discrete illumination sources across both visible and near-infrared ranges. Characterizing these emission profiles ensures that each wavelength is spectrally distinct and properly aligned for multispectral imaging of skin features at varying depths. The goal of this testing was to confirm that the illumination subsystem delivers stable, well-defined wavelength bands suitable for inclusive skin imaging.

Data Analysis — The optical and electrical characteristics of each LED were tested using a function and arbitrary waveform generator to provide precise voltage and current control. Each LED channel was powered individually at its forward voltage and current from DigiKey listed specifications. The visible wavelength LEDs are 470 nm (blue), 525 nm (green), 630 nm (red), and white (broad-spectrum). The visible wavelengths were tested with a forward current of 20 milliamperes. The near-infrared LEDs at 850 nm and 940 nm were operated at a DC forward current of 100 milliamperes to achieve measurable emission within the spectrometer's detection range.

A High-Resolution Spectrometer from Ocean Optics was used to capture the emission spectra of each LED. The spectrometer's input fiber was aligned directly with the optical axis of each LED at a fixed distance to maintain uniform coupling efficiency. For the high-intensity visible and white LEDs, a polarizer and adjustable aperture were inserted in front of the LED assembly to reduce intensity and minimize detector saturation. Each LED was activated individually to eliminate spectral overlap, and the measurements were recorded under identical geometric and optical conditions for all channels.

Results — The spectral profiles obtained from the HR2000CG-UV-NIR spectrometer confirmed that each LED emitted at its expected nominal wavelength with minimal deviation. The blue, green, and red LEDs produced narrow emission bands separated by more than 100 nanometers between peaks, demonstrating minimal spectral overlap across the visible range.

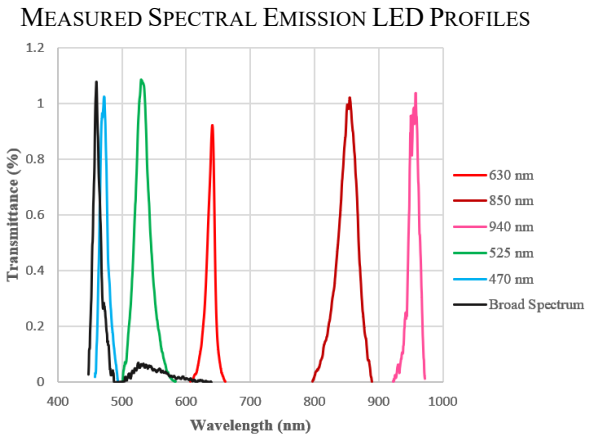

Fig. 9. The measured data was used to generate the converter efficiency profile as a function of output current.

The white LED showed a broad emission from about 430 to 650 nm, with a strong peak near 450 nm from the phosphor conversion process, giving a neutral color temperature and uniform illumination for baseline imaging. As shown in figure 9, each LED has distinct spectral peaks. The near-infrared LEDs peaked at 850 and 940 nm, extending into the 600–1300 nm therapeutic window, allowing deeper light penetration where melanin absorption is lower and scattering dominates, confirming effective multispectral illumination for surface and subsurface imaging.

Conclusions — The multispectral LED testing confirmed that all illumination channels met expected

optical and electrical parameters. Each LED maintained stable emission, accurate wavelength alignment, and consistent intensity at its rated current. The adjustable polarizer and aperture ensured precise spectral capture and prevented detector saturation. As a multispectral system, SkinLumina captures surface and deeper structures with high contrast, enhancing tissue visibility and supporting biomedical imaging applications.

C. Visible and Near-Infrared (NIR) Penetration Depth

This section calculates the optical penetration depths of visible and near-infrared light in the synthetic skin phantoms. The analysis uses India ink absorption and titanium dioxide scattering to estimate light attenuation through the material. These parameters define how deeply each wavelength penetrates skin-like tissue. Results show shorter wavelengths are absorbed near the surface, while longer ones reach deeper layers, guiding the layered phantom design for imaging validation.

Data Analysis — The absorption behavior of the artificial skin phantom was modeled using India ink as a broadband absorber dispersed in the silicone material. The relationship between the absorption coefficient and ink concentration follows the expression

$$\boldsymbol{\mu_a(\lambda) = \varepsilon_{a,ink}(\lambda) \times C_{ink}} \tag{3}$$

The absorption coefficient $\mu_a(\lambda)$ represents light absorption at wavelength λ, where $\varepsilon_{a,ink}(\lambda)$ is the specific absorption of India ink. C_{ink} is the fractional concentration of ink in the mixture. The dermis used 100 g of silicone with 0.46 g of ink, and the epidermis used 20 g of silicone with 0.092 g of ink. Since Cink remained constant, its effect was negligible in the wavelength-dependent analysis.

TABLE III
ABSORPTION COEFFICIENT APPROXIMATIONS

λ (nm)	$\varepsilon_{a,ink}(\lambda)$ (mm^{-1} per %)	C_{ink}	μ_a(mm^{-1})
470	25	0.0046	0.115
530	18	0.0046	0.083
630	10	0.0046	0.046
850	2.5	0.0046	0.012
940	2.0	0.0046	0.009

Values of $\varepsilon_{a,ink}(\lambda)$ in table III were approximated from published measurements of the India ink absorption spectra reported by Di Ninni et al. (2010) and Madsen et al. (1992). [2],[3] These sources provide spectral dependence of India ink's absorption, which decreases progressively from the visible to near-infrared range. Applying these approximations allowed estimation of $\mu_a(\lambda)$ for each illumination wavelength used in SkinLumina. The resulting trend confirms that absorption decreases by roughly a factor of five from 470 nm to the NIR wavelengths, consistent with the expected optical response of biological skin layers.

The scattering behavior of the artificial skin phantom, $\mu_s'(\lambda)$, was modeled using titanium dioxide (TiO_2) as the main scattering agent dispersed in the silicone mixture. The reduced scattering coefficient was approximated using the combined relationship

$$\mu_s'(\lambda) = \mu_s(\lambda)(1-g) = A(1-g)\left(\frac{\lambda}{\lambda_0}\right)^{-b} \tag{4}$$

As seen in equation (2), A is a proportionality constant determined by the TiO_2 concentration. The anisotrophy factor, g, is determined to be approximately 0.8–0.9, representing forward-directed scattering within the silicon samples. The reference wavelength, λ_0, was set to 500 nm. The coefficient, b, in (4) represents the wavelength-dependent scattering slope. This typically ranges from 0.7 to 1.2 for TiO_2. [4]

In this phantom, TiO_2 was added at a fixed concentration of approximately about 1 gram of TiO_2 powder per 100 grams of total silicone base. Using this approximation, the reduced scattering coefficients (μ_s') were estimated at each LED wavelength. The results follow the expected inverse wavelength dependence where scattering is strongest in the blue LED region and decreases steadily toward the near-infrared, allowing for deeper light penetration at longer wavelengths.

We applied the measured absorption and scattering coefficients of the skin samples to the penetration depth equation to calculate how deeply light travels through the material. The penetration depth is defined with:

$$\delta = \frac{1}{\sqrt{3\mu_a(\mu_a + \mu_s')}} \tag{5}$$

Equation (5) combines the effects of absorption μ_a and reduced scattering μ_s' to describe how light travels through the material at different wavelengths. [4]

Results — Greater absorption or scattering results in a smaller penetration depth, keeping light closer to the surface, while smaller values allow light to reach deeper layers. Applying this relationship to each LED and NIR wavelength shows that shorter visible wavelengths penetrate less deeply within the phantom, whereas longer near-infrared wavelengths reach farther.

The results in table IV confirm the expected optical behavior of the SkinLumina phantom and demonstrate the

device's ability to separate surface and subsurface features using multispectral illumination.

TABLE IV
ESTIMATED PHANTOM PENETRATION DEPTHS

λ (nm)	μ_a (mm^{-1})	μ_s' (mm^{-1})	δ (mm)
470	0.115	2.5	1.05
530	0.083	2.0	1.39
630	0.046	1.5	2.17
850	0.012	1.0	5.26
940	0.009	0.9	6.37

Conclusions — The penetration depth calculations modeled how visible and near-infrared light moves through skin-like materials. Shorter wavelengths were absorbed and scattered near the surface, while longer wavelengths penetrated several millimeters deeper. These results confirm that the silicone mixtures accurately mimic light transport in biological tissue and guided the design of the three-layer skin phantom and LED wavelength selection.

D. Spatial Resolution Analysis

The spatial resolution test was performed to evaluate the optical performance and image sharpness of the SkinLumina system. Accurate spatial resolution ensures that small surface and subsurface skin features can be clearly resolved and correctly identified. This analysis determines how effectively the imaging system transfers fine detail from the sample to the captured image, validating the optical alignment and focus quality of the prototype.

Data Analysis — Spatial resolution was measured using a custom Python tool with a graphical interface. The user loads an image, defines a circular ROI, and analyzes resolution metrics. Using OpenCV, the image is converted to grayscale, filtered to reduce noise, and sampled horizontally and vertically through the selected feature center.

From these line profiles, the software calculates three key spatial resolution metrics:

(1) Full Width at Half Maximum (FWHM): quantifies the apparent width of a feature, indicating the degree of edge sharpness or blur.
(2) Edge Width: measures the pixel distance over which intensity rises from 10% to 90% of its maximum value, providing another measure of edge definition.
(3) MTF50 (Modulation Transfer Function 50%): represents the spatial frequency at which image contrast falls to half its original value, serving as a reliable indicator of perceived image sharpness.

The algorithm also estimates feature size by fitting contours to the target using ellipse or circle fitting. All computed values, including feature diameter and edge sharpness, can be exported to a data file for further analysis.

Results — As seen in figure 10, as image blur increases, the FWHM broadens and the system's spatial frequency response decreases, indicating reduced image sharpness.

FWHM VS. MTF50 SPATIAL FREQUENCY

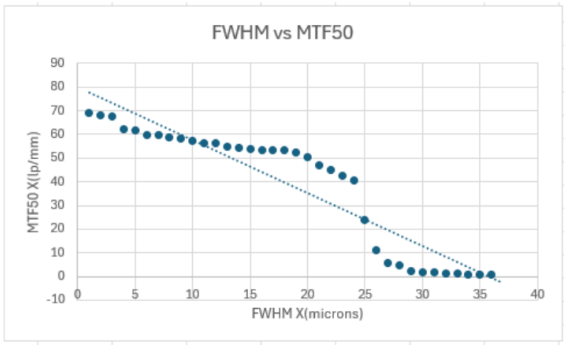

Fig. 10. The chart illustrates the inverse relationship between the full width at half maximum (FWHM) of the point spread function and the MTF50 spatial frequency.

The results from figure 11 indicate consistent MTF50 values from the center (r = 0) to the periphery (r = 1), demonstrating minimal field curvature and precise optical alignment.

RADIAL SPATIAL RESOLUTION

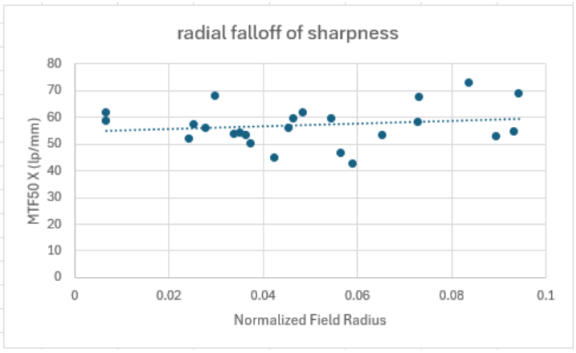

Fig. 11. The chart illustrates the radial falloff of image sharpness, showing how spatial resolution varies with distance from the image center.

Conclusions — The spatial resolution analysis verified that SkinLumina maintains consistent image sharpness and contrast across the entire imaging field. The inverse FWHM–MTF50 relationship and uniform radial resolution confirm precise optical alignment and minimal aberration, validating the system's ability to resolve fine skin features accurately.

E. Hexadecimal Color Detection Analysis

A hexadecimal (HEX) color code represents a color using six digits derived from red, green, and blue (RGB) pixel values. In the SkinLumina system, this code quantifies skin reflectance, allowing real-time LED adjustments for consistent illumination across diverse skin tones and ensuring inclusive imaging performance.

Data Analysis — The system uses OpenCV and NumPy to extract the center pixel and its surrounding neighborhood from each captured image. The RGB intensity values are averaged to reduce noise and converted into a six-digit HEX color code representing the dominant skin reflectance.

Results — As shown in figure K, detection times ranged from 140 to 280 milliseconds with minimal variation across samples. Repeated testing demonstrated 95% consistency in color detection across ten trials under controlled lighting conditions as seen in figure 12.

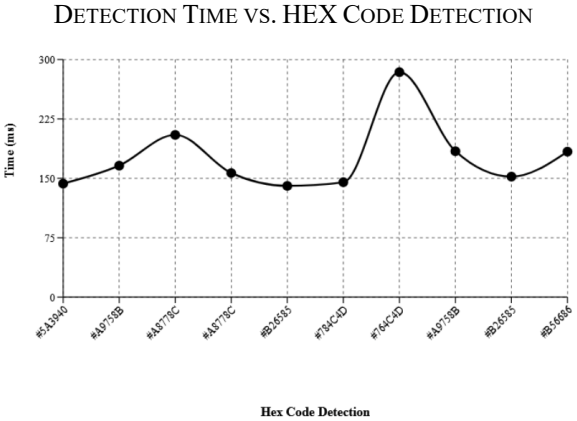

Fig. 12. The chart shows detection time and consistency of HEX color extraction across captured images.

Conclusions — The HEX color detection process provides a fast and reliable measure of skin reflectance, allowing the system to adapt LED intensity and color balance for uniform spectral imaging and more inclusive diagnostic performance.

VI. CONCLUSION

The SkinLumina system successfully demonstrates a compact, adaptive multispectral imaging platform designed to improve inclusivity in dermatological analysis. Through the integration of visible and near-infrared illumination, polarization control, and real-time spectral calibration, the device provides clear imaging of both surface and subsurface skin features across a range of skin tones. Experimental validation confirmed consistent optical alignment, reliable power regulation, and accurate wavelength control. Overall, SkinLumina achieves its goal of enabling equitable, high-fidelity skin imaging that supports early detection and unbiased dermatological assessment.

ACKNOWLEDGEMENT

The team thanks to the SkinLumina review committee, especially Dr. Aristide Dogariu and Dr. Peter Delfyett for their guidance in optical testing and project direction, and Dr. David Weinstein for his insight into current dermatological practices and skin cancer diagnostics.

REFERENCES

[1] Matsushita, Teruo. Electricity: Electromagnetism and Electric Circuits. 1st ed. Cham: Springer, 2024. Web.

[2] Ninni, Paola & Martelli, Fabrizio & Zaccanti, Giovanni. (2010). The use of India ink in tissue-simulating phantoms. Optics Express. 18. 26854-26865. 10.1364/OE.18.026854.

[3] Portesi, Chiara & Mijatovic, D & Veldhuis, D & Brinkman, A & Monticone, E. & Gonnelli, R. (2006). MgB2 magnetometer with a directly coupled pick-up loop. Superconductor Science and Technology. 19. S303. 10.1088/0953-2048/19/5/S29.

[4] Steven L. Jacques, Brian W. Pogue, "Tutorial on diffuse light transport," J. Biomed. Opt. 13(4) 041302 (1 July 2008) https://doi.org/10.1117/1.2967535